

Diving into Darkness: A Dual-Modulated Framework for High-Fidelity Super-Resolution in Ultra-Dark Environments

Jiaxin Gao¹, Ziyu Yue², Yaohua Liu¹, Sihan Xie¹, Xin Fan¹, Risheng Liu¹

¹ School of Software Technology, Dalian University of Technology, China

² School of Mathematical Science, Dalian University of Technology, China

Jiaxinn.gao@outlook.com, 11901015@mail.dlut.edu.cn, liuyaohua_918@163.com, XSH2018@mail.dlut.edu.cn, xin.fan@dlut.edu.cn, rslu@dlut.edu.cn

Abstract

Super-resolution tasks oriented to images captured in ultra-dark environments is a practical yet challenging problem that has received little attention. Due to uneven illumination and low signal-to-noise ratio in dark environments, a multitude of problems such as lack of detail and color distortion may be magnified in the super-resolution process compared to normal-lighting environments. Consequently, conventional low-light enhancement or super-resolution methods, whether applied individually or in a cascaded manner for such problem, often encounter limitations in recovering luminance, color fidelity, and intricate details. To conquer these issues, this paper proposes a specialized dual-modulated learning framework that, for the first time, attempts to deeply dissect the nature of the low-light super-resolution task. Leveraging natural image color characteristics, we introduce a self-regularized luminance constraint as a prior for addressing uneven lighting. Expanding on this, we develop Illuminance-Semantic Dual Modulation (ISDM) components to enhance feature-level preservation of illumination and color details. Besides, instead of deploying naive up-sampling strategies, we design the Resolution-Sensitive Merging Up-sampler (RSMU) module that brings together different sampling modalities as substrates, effectively mitigating the presence of artifacts and halos. Comprehensive experiments showcases the applicability and generalizability of our approach to diverse and challenging ultra-low-light conditions, outperforming state-of-the-art methods with a notable improvement (i.e., $\uparrow 5\%$ in PSNR, and $\uparrow 43\%$ in LPIPS). Especially noteworthy is the 19-fold increase in the RMSE score, underscoring our method’s exceptional generalization across different darkness levels. The code will be available online upon publication of the paper.

Introduction

Image super-resolution is a classical problem in low-level vision. Nevertheless, research towards Low-Light Image Super-Resolution (LLISR) has been relatively neglected, despite its practical importance for applications such as surveillance, automated driving, and medical image analysis. This study aims to explore the enhancement of low-resolution images captured under ultra-dark conditions to achieve both brightness adjustment and magnification, and ultimately generates high-resolution clear images with normal illumination.

In comparison to well-lit scenarios, the super-resolution process can amplify a range of issues arising from low-light

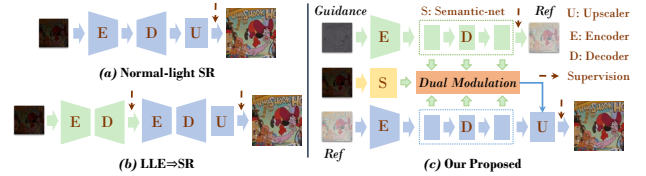


Figure 1: Comparative illustration showcasing the fundamental architectures towards LLISR of various solutions.

conditions, such as inadequate details and color distortion due to uneven illumination. Typically, illumination distribution is uneven in dimly lit environments, potentially resulting in pronounced shadows and highlight regions. Hence, handling these lighting variations is essential during super-resolution to ensure increased resolution while retaining illumination details. Moreover, due to shooting in low-light conditions, missing details may result in inaccurate or numerous artifacts and halos in the super-resolution results.

Evidently, it has been confirmed by extensive experiments that current methods designed for low-light image enhancement (LLE) and normal-light image super-resolution (SR) exhibit noticeable limitations in solving the LLISR problem. Furthermore, simply applying these task-specific models in a cascaded manner (e.g., LLE \Rightarrow SR) still fails to yield satisfactory results. The aforementioned findings have been extensively discussed in the literature (Aakerberg, Nasrollahi, and Moeslund 2021). *Figure 1* illustrates the qualitative and quantitative outcomes of various schemes (a-c) for handling LLISR tasks. It is important to emphasize that all the methods involved have been retrained on the specific RELISUR dataset (Aakerberg, Nasrollahi, and Moeslund 2021). As illustrated in *Figure 2*, the normal-light SR technique HAT (Chen et al. 2023) fails to reconstruct the fine details of low-light input images, resulting in significant artifacts. The LLE method LLFormer (Wang et al. 2023) cascaded with HAT exhibits noticeable color shifts and unclear textures. In comparison, our proposed method shows more natural and realistic colors and structural details. For further comparative analysis results, please refer to the Experimental Section.

To address these issues, this paper proposes a specialized low-light super-resolution paradigm for simultaneously **Brightening** and **Magnifying** low-resolution images captured in **Ultra-dark** scenes, dubbed **UltraBM**. UltraBM utilizes

a dual-stream learning framework, which represents a pioneering effort to comprehensively analyze the essence of the LLISR task. During the initial stage, we propose incorporating illumination prior to impose constraints on low-light scenes in an unsupervised manner. Whereas, in the subsequent stage, we introduce a semantic knowledge base, and build Illumination-Semantic Dual Modulation (ISDM) as refinement middleware. ISDM runs through the entire network layer of decoding for cross-branch interaction, facilitating the far-flung retention of illuminance details and semantic color details, to enable the super-resolution network to focus more on faithful texture details. Furthermore, we introduce a Resolution-Sensitive Merging Up-sampler (RSMU) module, a strategic departure from naive up-sampling, effectively alleviating artifacts and halos. We conducted extensive experiments to validate the effectiveness of the proposed method. The main contributions can be summarized as follows:

- Aiming for the highly-coupled complex task of simultaneously brightening and magnifying images captured in ultra-dark scenes, we introduce a tailored high-fidelity super-resolution framework dubbed UltraBM, marking a novel attempt to deeply dissect the nature of the LLISR task and proved feasible solution strategies.
- To uphold illuminance details while enhancing resolution, we model low-light scenes by imposing principled priors as initial constraints. And further we construct a refinement middleware, Illumination-Semantic Dual Modulation (ISDM) that operates in a top-down manner to modulate reflection features, which effectively avoids exacerbating color distortions and emphasizes faithful texture details.
- Instead of employing naive up-sampling rules, we assemble different sampling modalities as substrates, thereby architecting a Resolution-Sensitive Merging Up-sampler (RSMU) that adeptly mitigates artifacts and halos, particularly tailored for the refinement of high-fidelity images.

We evaluate the applicability and generalizability of the proposed method in diverse extremely ultra-dark scenes, and demonstrate its strengths through comprehensive analysis.

Related Work

Low-Light Image Enhancement

LLE aims to make images hidden in the dark visible. The most widely circulated model is based on the Retinex theory of separating illumination and reflection image layers for reconstruction (Wei et al. 2018; Wang et al. 2019; Zhang, Zhang, and Guo 2019; Ren et al. 2020; Gao et al. 2023; Liu et al. 2021). In recent years, great progress has also been made in designing models based on convolutional neural networks (Hira et al. 2021; Li et al. 2017; Yang et al. 2020a; Jiang et al. 2021; Wang et al. 2018a). For example, ZeroDCE (Li, Guo, and Loy 2021) achieved effective enhancement of low-light images by learning reference-free histogram stretching and enhancement functions. Recently, an unsupervised method SCI was proposed in (Ma et al. 2022) to use a basic illuminance learning module to improve the low-light scene generalization ability. LLFormer (Wang

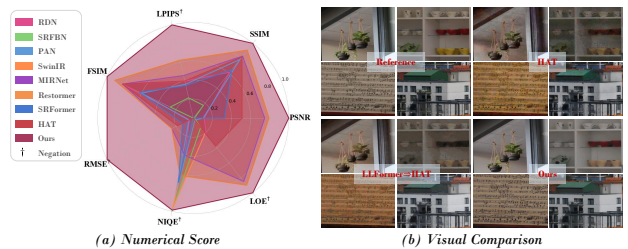


Figure 2: Comparisons among different schemes for LLISR in terms of numerical scores (a), as well as visualization results (b). A recent LLE method (i.e., LLFormer (Wang et al. 2023)), and a normal-light SR method (HAT (Chen et al. 2023)), are presented as examples for visualization.

et al. 2023) utilized a transformer-based approach with axis-based multi-head self-attention and cross-layer attention fusion block to effectively enhance low-light images. Although the aforementioned methods perform well in the LLE task, their direct concatenation with normal-light SR techniques for the LLISR task shows evident limitations.

Normal-light Image Super-Resolution

Normal-light SR task involves generating high-resolution images from low-resolution inputs under standard lighting conditions. In recent decades, a large number of methods based on convolutional neural networks have emerged to continuously refresh the performance (Zhang et al. 2018b; Li et al. 2019; Zhao et al. 2020; Haris, Shakhnarovich, and Ukita 2018; Wang et al. 2018b). It is worth noting that Zamir *et al.* (Zamir et al. 2020) proposed the image restoration architecture with a non-local attention mechanism and multi-scale feature aggregation, which demonstrates remarkable performance in normal-light SR tasks. Recently, benefiting from the surge of self-attention mechanisms, various transformer-based approaches have been developed for super-resolution enhancement. Among these, notable approaches include SwinIR (Liang et al. 2021), Restormer (Zamir et al. 2022a), the recently proposed SRFormer (Zhou et al. 2023) and HAT (Chen et al. 2023). However, these methods tailored for normal lighting conditions fail to address the challenges posed by low-light environments, often resulting in undesirable outcomes such as artifact spreading and texture blurring.

Methodology

Focusing on LLISR, this paper aims to establish an end-to-end learning framework for recovering a normal-light super-resolution image (i.e., y^{NS}) from a given low-resolution image captured in low-light environments (i.e., x^{LL}). The crux of this approach lies in simultaneously learning brightness enhancement while ensuring an elevation in resolution. To tackle this issue effectively, we introduce a tailored low-light super-resolution framework for LLISR, dubbed UltraBM. In what follows, we detail the proposed method.

Retinex-Inspired Dual-stream Framework

Drawing inspiration from the classical Retinex theory, we initially construct a foundational illumination learning net-

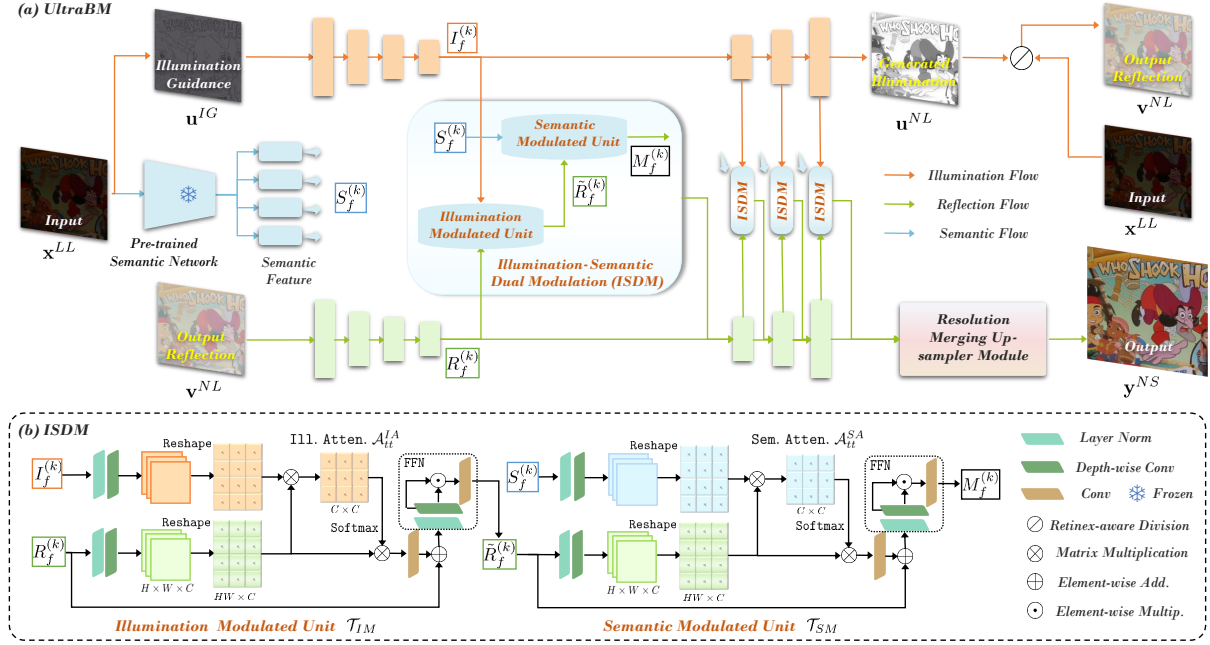


Figure 3: (a): The overview of the proposed UltraBM. Given low-light low-resolution image \mathbf{x}^{LL} , we construct the dual-stream framework to generate the initial reflection image \mathbf{v}^{NL} with illumination guidance \mathbf{u}^{IG} . Subsequently, \mathbf{v}^{NL} is fed into a subsequent refinement super-resolution network to restore a normal-light, super-resolution image \mathbf{y}^{NS} . (b) shows the refinement middleware, ISDM, which top-down modulates reflection features across branches to facilitate interactions.

work to capture the underlying physical principles of low-light scenes. As illustrated in *Figure 3 (a)*, we introduce a neighborhood difference operator F_{diff} following (Ma et al. 2021) to compute the initial illumination guidance $\mathbf{u}^{IG} = F_{diff}(\mathbf{x}^{LL})$. Subsequently, \mathbf{u}^{IG} is fed into a U-Net-style network to generate the illumination map \mathbf{u}^{NL} , with such learning process being supervised by the introduced scene constraint for ultra-dark environments¹. Further, we obtain the low-resolution reflection map \mathbf{v}^{NL} by employing the Retinex-based element-wise division, formulated as

$$\mathbf{v}^{NL} = \mathbf{x}^{LL} \oslash \mathbf{u}^{NL}, \mathbf{u}^{NL} = U_{net}(\mathbf{u}^{IG}). \quad (1)$$

In the subsequent stage, \mathbf{v}^{NL} is transmitted to another U-Net-style network with similar architecture to complete refined super-resolution process. Inspired by self-attention mechanisms (Zamir et al. 2022a), we design a refined intermediary, namely Illumination-Semantic Dual Modulation (ISDM), depicted as the blue shaded box in *Figure 3 (b)*, positioned within the decoding stage to facilitate progressive inter-branch interactions. Experiments confirm that ISDM can effectively avoid exacerbating color shifts and distortions during image super-resolution. Finally, we devised a Resolution-Sensitive Merging Up-sampler (RSMU) module to obtain the enhanced image \mathbf{y}^{NS} . It is worth noting that the U-Net is constructed based on Context Units (CUs, see *Figure 4 (c)*) as the base module, which transforms the scale using Maxpooling and bilinear up-sampling operations in the encoding and decoding phases, respectively².

¹Please refer to constraint losses as outlined in Eqs. (6)-(7).

²Refer to the Supplementary Material for detailed architectures.

In the following, we expand on the architectural details of two key modules designed, including ISDM and RSMU.

Illumination-Semantic Dual Modulation

As shown in (a) of *Figure 3*, the ISDM consists of the Illumination Modulated Unit (IMU, \mathcal{T}_{IM}) and Semantic Modulated Unit (SMU, \mathcal{T}_{SM}) with a similar architectural design. The illumination features and reflection features extracted from the decoders of the top and down branches are denoted as $I_f^{(k)}$ and $R_f^{(k)}$, respectively. $k \in \{1, 2, \dots, 5\}$ indexes the feature level. Inspired by the fact that large semantic knowledge base can improve the network’s representational capabilities, we utilize a pre-trained semantic network HRNet (Wang et al. 2020) to extract multi-scale semantic features $S_f^{(k)}$ from \mathbf{x}^{LL} .

The ISDM facilitates a top-down information flow of illumination and semantic features, and calculates a similarity matrix as modulation response to guide the refinement of reflection features. The structural details of ISDM are depicted in *Figure 3 (b)*. Specifically, $I_f^{(k)}$ and $R_f^{(k)}$ are individually transformed through layer normalization and depth-wise convolution, further reshaping to compute the illumination attention map $\mathcal{A}_{tt}^{IA} \in \mathcal{R}^{C \times C}$, presented by

$$\mathcal{A}_{tt}^{IA} = LN(Conv(I_f^{(k)})) \otimes LN(Conv(R_f^{(k)})). \quad (2)$$

Then \mathcal{A}_{tt}^{IA} is normalized through the softmax function and update $R_f^{(k)}$ in a dynamic weighting manner, and a feed-forward network ψ_{FFN} followed by (Zamir et al. 2022a) is

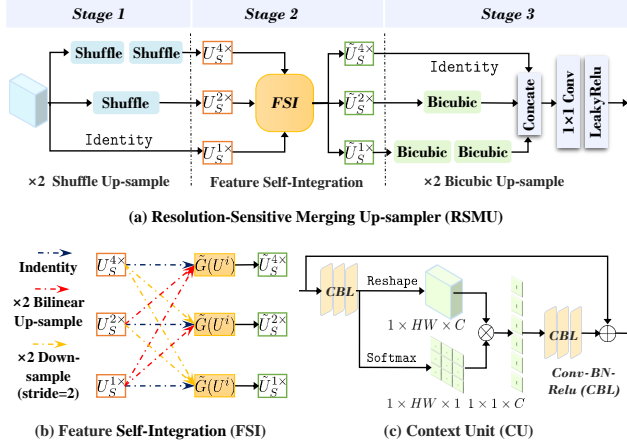


Figure 4: Illustrations of RSMU (a), FSI (b) and CU (c).

introduced for further content reconstruction, expressed as

$$\mathcal{T}_{IM} = \psi_{FFN} (\mathcal{S} [A_{tt}^{IA} \otimes \text{Conv} (R_f^{(k)})]), \quad (3)$$

where \mathcal{S} is the Sigmoid function, and \otimes denotes the element-wise multiplication operation. Thus we obtain the modulated reflection features $\tilde{R}_f^{(k)} = \mathcal{T}_{IM}(I_f^{(k)}, R_f^{(k)})$. Similarly, $\tilde{R}_f^{(k)}$ is fed into the proposed \mathcal{M}^{SMU} to generate the semantic attention map $\mathcal{A}_{tt}^{SA} \in \mathcal{R}^{C \times C}$, followed by

$$\mathcal{T}_{SM} = \psi_{FFN} (\mathcal{S} [A_{tt}^{SA} \otimes \text{Conv} (\tilde{R}_f^{(k)})]), \quad (4)$$

where $\mathcal{A}_{tt}^{SA} = \text{LN} (\text{Conv} (S_f^{(k)})) \otimes \text{LN} (\text{Conv} (\tilde{R}_f^{(k)}))$. The doubly modulated feature $M_f^{(k)} = \mathcal{T}_{SM}(S_f^{(k)}, \tilde{R}_f^{(k)})$ is then propagated to the $k + 1$ decoding layer.

Resolution-Sensitive Merging Up-sampler

Typically, most of the normal-light SR methods employ naive up-sampling techniques (e.g., Bilinear (Zhang et al. 2018a) or Bicubic), which lack the ability to fully exploit the collaborative potential of scale-sensitive features. As a consequence, these methods face challenges in reproducing intricate high-quality details, undesirable artifacts and halos. Motivated by this, we construct the RSMU module that amalgamates distinct sampling modalities as foundational constituents to progressively learn the mapping from low-resolution space to high-resolution space.

As illustrated in Figure 4 (a), RSMU comprises three stages, each employing different sampling modalities as substrates, including pixel shuffle up-sampling, bilinear up-sampling, and bicubic up-sampling. Initially, it employs pixel shuffle in parallel to generate three separate scale features $U_S^{i \times}$, where $i \in \{1, 2, 4\}$ indexes the scale layer. Subsequently, these three sets of distinct features are converged within the Feature Self-Integration (FSI) module for both feature selection and fusion. As depicted in Figure 4 (b), FSI aggregates and transforms the input features $U_S^{i \times}$, yielding corresponding outputs denoted as $\tilde{U}_S^{j \times}$, where j takes values from $\{1, 2, 4\}$ to represent different output resolution levels.

Through the introduced selective attention mechanism (Zamir et al. 2022b), denoted as \mathcal{M}_{skff} , each $\tilde{U}_S^{j \times}$ dynamically selects essential features, which can be formalized as follows:

$$\tilde{U}_S^{j \times} = [\tilde{G}(U_S^{i \times})]_{i=1,2,4}, \quad \tilde{G} = \mathcal{M}_{skff} \circ \begin{cases} 1 & \forall i = j, \\ \uparrow & \forall j > i, \\ \downarrow & \forall j < i. \end{cases} \quad (5)$$

In the specific mathematical form of \tilde{G} : when $i = j$, an Identity operation (with unchanged size) is used (blue dashed line); when $j < i$, a transposed convolution down-sampling with a stride of 2 is employed (yellow dashed line); when $j > i$, bilinear up-sampling is used (red dashed line).

Loss Function

Self-regularized Luminance Loss. Inspired by the color statistical regularities of natural image distributions, we propose the self-regularized luminance loss \mathcal{L}_{SL} , to encourage the naturalness of colors for \mathbf{v}^{NL} , which can be formulated as

$$\mathcal{L}_{SL}(\mathbf{v}^{NL}) = e^{|\bar{\mathbf{v}}_c^{NL} - \mu_c - \sigma_c|} - 1, \quad c \in \{R, G, B\}, \quad (6)$$

where μ_c and σ_c denote mean and standard deviation of the natural image distribution of Imagenet (Deng et al. 2009), with $\mu_c = [0.485, 0.456, 0.406]$ and $\sigma_c = [0.229, 0.224, 0.225]$. $\bar{\mathbf{v}}^{NL}$ denotes the channel-wise mean.

Illumination Smooth Loss. Drawing insights from (Ma et al. 2021), we utilize the $\text{Smooth}_{\mathcal{L}_1}$ loss to ensure the structural consistency between the generated illuminance image \mathbf{u}^{NL} and the gray image \mathbf{x}_G^{LL} of input, presented as

$$\mathcal{L}_{IS}(\mathbf{u}^{NL}, \mathbf{x}_G^{LL}) = \text{Smooth}_{\mathcal{L}_1}(\mathbf{u}^{NL} - \mathbf{x}_G^{LL}), \quad (7)$$

where $\text{Smooth}_{\mathcal{L}_1}(x) = 0.5x^2$ when $|x| \leq 1$; otherwise, $\text{Smooth}_{\mathcal{L}_1}(x) = |x| - 0.5$.

Reconstruction Loss. To maintain the content consistency between the generated image \mathbf{y}^{NS} and the reference image (normal-light high-resolution image) \mathbf{y}^{NH} , we introduce the reconstruction loss, i.e.,

$$\mathcal{L}_R(\mathbf{y}^{NS}, \mathbf{y}^{NH}) = \|\mathbf{y}^{NS} - \mathbf{y}^{NH}\|_1, \quad (8)$$

Perceptual Loss. To maintain perceptual consistency, we introduce perceptual loss (Johnson, Alahi, and Fei-Fei 2016) to calculate the disparity between \mathbf{y}^{NS} and \mathbf{y}^{NH} :

$$\mathcal{L}_P(\mathbf{y}^{NS}, \mathbf{y}^{NH}) = \frac{1}{c_j h_j w_j} \|\phi_j(\mathbf{y}^{NS}) - \phi_j(\mathbf{y}^{NH})\|_1, \quad (9)$$

where ϕ is the VGG-19 model, $c_j h_j w_j$ denotes the size of the feature map at the j -th layer. We use $\{\text{conv1}, \dots, \text{conv5}\}$ feature layers with weights $\{0.1, 0.1, 1, 1, 1\}$.

Overall Loss. We train our network by minimizing the following overall loss:

$$\mathcal{L}_{total} = \lambda_1 * \mathcal{L}_{SL} + \lambda_2 * \mathcal{L}_{IS} + \lambda_3 * \mathcal{L}_R + \lambda_4 * \mathcal{L}_P, \quad (10)$$

where the weights $\{\lambda_i\}_{i=1}^4$ are set to 1.0, 1.0, 1.0, 1.2.

Experiments

Dataset and Experimental Settings

Dataset. We evaluate the performance on two widely-used datasets: RELLISUR³ and DarkFace (Yang et al. 2020b)⁴.

³<https://vap.aau.dk/rellisur/>

⁴<https://flyywh.github.io/CVPRW2019LowLight/>

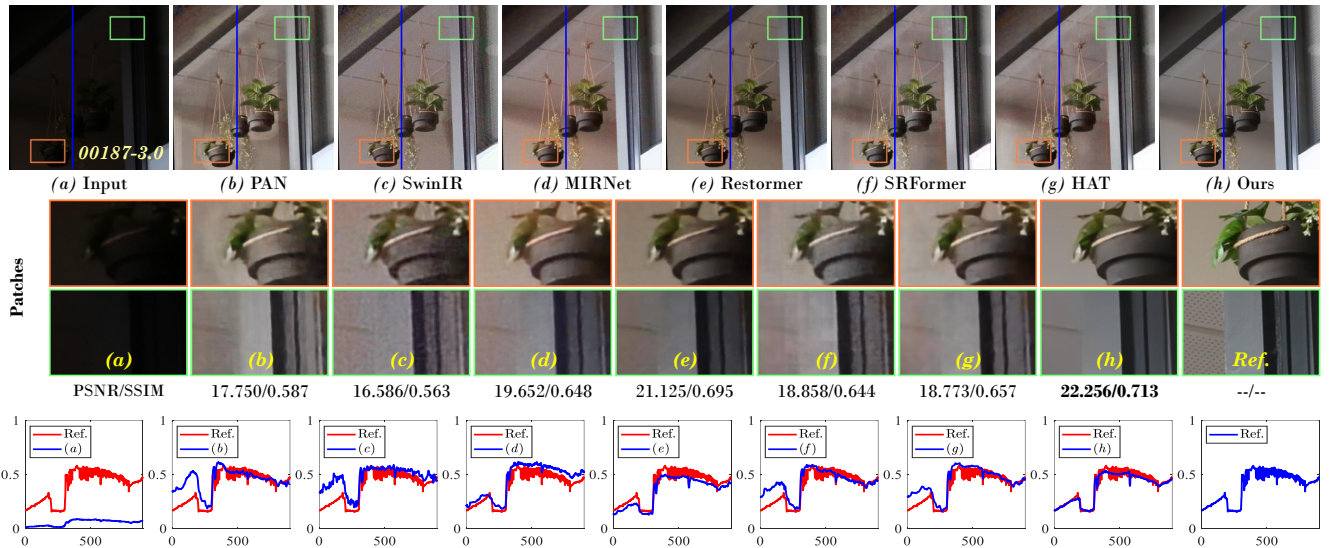


Figure 5: Qualitative comparisons on RELLISUR dataset of our method with SOTA methods for 2x LLISR task. Below signal maps provide the differences of pixel intensity between generated images and the reference image along the blue line segment.

Metrics	RDN ^{18CVPR}	SRFBN ^{19CVPR}	PAN ^{20ECCV}	MIRNet ^{20ECCV}	SwinIR ^{21ICCV}	Restormer ^{22CVPR}	SRFormer ^{23ICCV}	HAT ^{23CVPR}	Ours
PSNR \uparrow	18.794/18.201	18.435/17.653	18.757/18.051	21.054/19.773	18.387/17.452	<u>21.217/20.290</u>	19.558/18.708	20.213/19.750	22.264/21.036
SSIM \uparrow	0.701/0.701	0.662/0.665	0.716/0.703	0.720/0.704	0.647/0.658	<u>0.727/0.720</u>	0.704/0.705	0.719/0.715	0.743/0.726
LPIPS \downarrow	0.455/0.584	0.510/0.640	0.465/0.567	0.436/0.599	0.577/0.686	<u>0.385/0.492</u>	0.469/0.613	0.454/0.561	0.254/0.371
RMSE \downarrow	0.120/0.128	0.125/0.136	0.119/0.129	<u>0.095/0.109</u>	0.125/0.139	<u>0.095/0.106</u>	0.110/0.430	0.103/0.110	0.005/0.006
NIQE \downarrow	7.864/9.098	7.202/7.766	7.370/8.737	7.881/8.803	7.231/9.489	7.636/9.065	7.550/9.664	8.332/10.028	7.216/7.537
LOE \downarrow	45.642/44.976	47.698/45.582	49.793/48.623	31.968/33.966	46.042/42.581	<u>30.889/30.856</u>	50.411/45.606	42.265/35.284	28.670/29.432

Table 1: Quantitative comparison among various normal-light SR methods on RELLISUR-Test dataset (i.e., 2x / 4x). The top-ranked and the second-ranked method are highlighted in bold and bold underlined, respectively.

Metrics	ZeroDCE ^{21TPAMI} \Rightarrow HAT ^{23CVPR} \ddagger	SCI ^{22CVPR} \Rightarrow HAT ^{23CVPR} \ddagger	LLFormer ^{23AAAI} \Rightarrow HAT ^{23CVPR} \ddagger
PSNR \uparrow	12.927/12.524	14.963/14.776	21.286/20.135
SSIM \uparrow	0.354/0.321	0.439/0.452	0.720/0.718
LPIPS \downarrow	0.698/0.739	0.591/0.697	0.455/0.575
RMSE \downarrow	0.015/0.019	0.200/0.205	0.093/0.105
NIQE \downarrow	7.389/8.132	7.625/8.235	8.574/9.231
LOE \downarrow	56.726/54.178	36.413/37.879	35.084/36.215

\dagger indicates training on 1x low-light RELLISUR dataset for LLE. \ddagger denotes training on 2x or 4x RELLISUR dataset for normal-light SR.

Table 2: Quantitative comparison among cascaded LLE \Rightarrow SR methods on RELLISUR dataset (i.e., 2x / 4x).

We utilize the RELLISUR dataset for training our method, since RELLISUR offers a collection of 1,045 image pairs at three distinct resolution scales (1x, 2x, and 4x) and five varying low-light levels (ranging from -2.5EV to -5.0EV), encompassing both low-resolution low-light images and high-resolution normal-light images.

Evaluation Metrics. We evaluate the performance using four

widely-used full-reference metrics, including pixel-wise Peak Signal to Noise Ratio (PSNR), Structural Similarity Index (SSIM), LPIPS (Agaian, Silver, and Panetta 2007) and Root Mean Square Error (RMSE), as well as two no-reference metrics Natural Image Quality Evaluator (NIQE) (Mittal, Soundararajan, and Bovik 2012) and LOE (Wang et al. 2013). **Implement Details.** All experiments were performed on a PC equipped with an NVIDIA GeForce GTX 2080Ti GPU, using the PyTorch 1.8.0 framework. Our model was trained using the Adam optimizer for a total of 150,000 iterations. The initial learning rate was set to 2×10^{-4} and the weight decay parameter is 1×10^{-4} with $\beta = [0.9, 0.999]$. The progressive training strategy with mini batch sizes sets to $[8, 5, 4, 2, 1, 1]$.

Comparisons with State-of-the-Art

We compare our method against two distinct schemes: normal-light SR methods and cascaded LLE \Rightarrow SR methods. To ensure a comprehensive comparison, we meticulously selected three representative LLE methods, including ZeroDCE (Li, Guo, and Loy 2021), SCI (Ma et al. 2022), and LLFormer (Wang et al. 2023), and eight normal-light SR methods, i.e., RDN (Zhang et al. 2018b), SRFBN (Li et al.

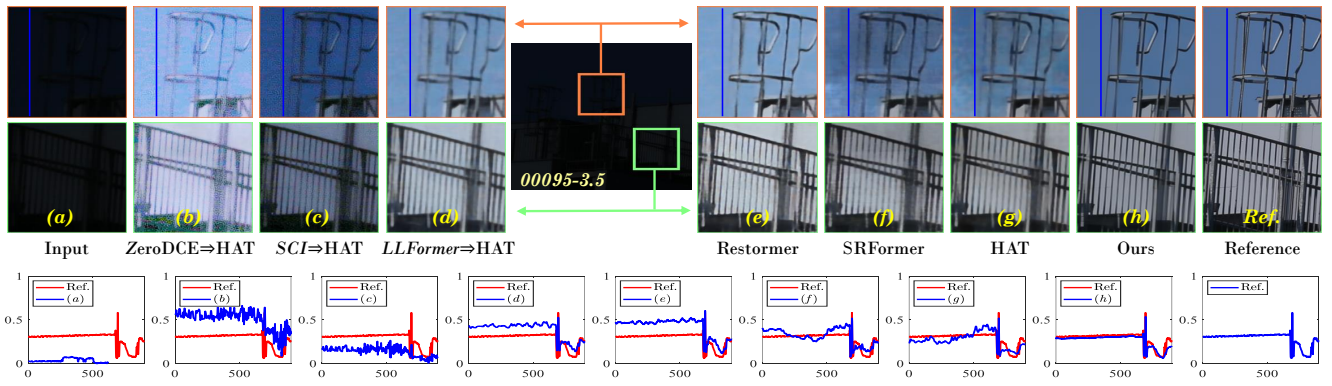


Figure 6: Qualitative comparisons on RELISUR dataset for 4x LLISR task. Below provides the differences of pixel intensity.

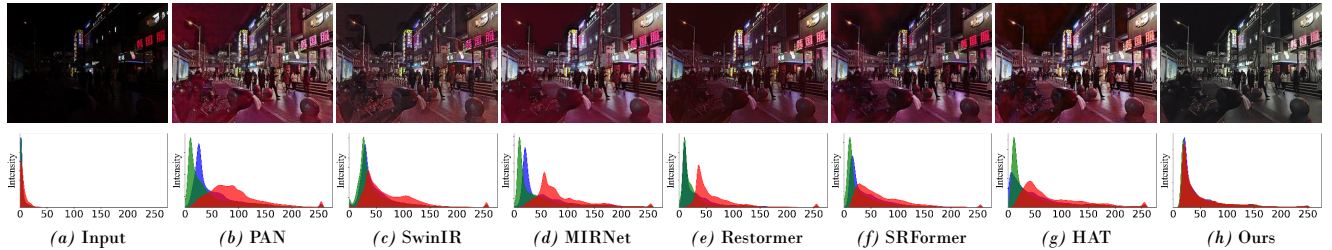


Figure 7: Visual comparison on DarkFace dataset for 2x LLISR task. Below is the probability density histogram about RGB.

2019), PAN (Zhao et al. 2020), SwinIR (Liang et al. 2021), and MIRNet (Zamir et al. 2020), Restormer (Zamir et al. 2022a), SRFormer (Zhou et al. 2023), HAT (Chen et al. 2023). We retrain all methods on RELISUR for fair comparisons.

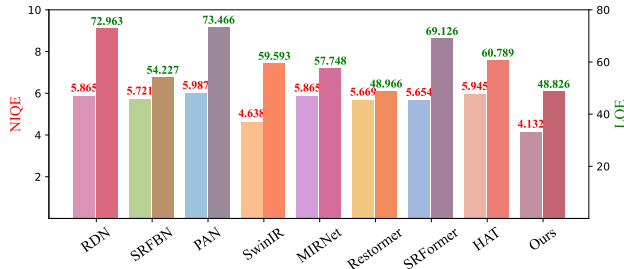


Figure 8: Generalization analysis on *DarkFace* dataset.

Metrics	SwinIR	Restormer	SRFormer	HAT	Ours
Params (MB)	11.683/11.825	26.126/26.209	10.162/10.220	9.473/9.621	69.561/69.687
FLOPs (G)	453.12/467.94	35.375/41.327	81.797/83.006	58.990/68.994	31.497/64.633
Infer. (S)	3.879/4.226	0.033/0.035	0.218/0.221	0.184/0.186	0.044/0.054

Table 3: Computational efficiency of SOTA methods (2x/4x).

LLE=>SR Methods. Among numerous SR methods, we have chosen the latest SR method, HAT^{23CVPR}, as the subsequent magnification model, cascaded behind three LLE methods. This setup allows us to observe the performance of the concatenated methods for the LLISR problem. Notably, consid-

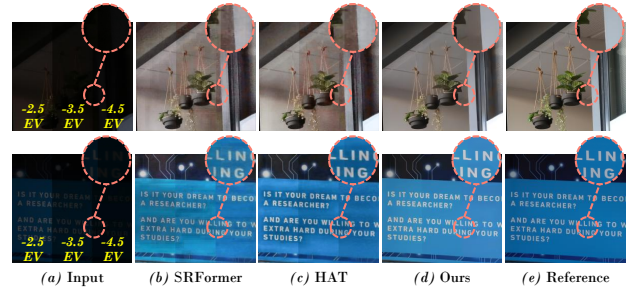


Figure 9: Generalization analysis across diverse darkness levels (ranging from -2.5EV to -4.5EV).

ering that ZeroDCE and SCI are unsupervised methods, we solely trained them on the 1x low-light RELISUR dataset for the preliminary brightening task. Additionally, as HAT serves as a posterior module, used for super-resolution on the brightened images, we trained the model on the 2x and 4x normal-light RELISUR datasets, denoting it as HAT_‡ to distinguish it from the original HAT.

Quantitative Evaluation. Tables 1 and 2 present the quantitative results among various normal-light SR methods and cascaded methods on the RELISUR dataset for 2x and 4x tasks. Our method outperforms existing state-of-the-art (SOTA) approaches, achieving the highest scores in six evaluation metrics. Compared to the closely ranked second-best Restormer, our approach achieved a significant improvement (i.e., $\uparrow 5\%$ in PSNR, $\uparrow 2\%$ in SSIM, and $\uparrow 50\%$ in LPIPS).

Configuration	PSNR \uparrow	SSIM \uparrow	LPIPS \downarrow
OS	20.213 $\downarrow_{0.051}$	0.676 $\downarrow_{0.067}$	0.316 $\uparrow_{0.062}$
DS (w/ x^{LL})	21.821 $\downarrow_{0.443}$	0.713 $\downarrow_{0.030}$	0.285 $\uparrow_{0.031}$
DS (w/ v^{LL})	22.264	0.743	0.254

Table 4: Exploring the performance comparison between one-stream (OS) and dual-stream (DS) architectures.

Qualitative Evaluation. Qualitative results on realistic *REL-LISUR* dataset are displayed in *Figures 5* and *6*. As illustrated, our method compared to other methods produces authentic images with vivid lightness, and an exceptional ability to recover high-frequency structural details. *Figure 7* displays visualization results on the *DarkFace-Test* dataset. Particularly noteworthy is our method’s exceptional performance in maintaining the natural authenticity of nighttime scenes.

Configuration	PSNR \uparrow	SSIM \uparrow	LPIPS \downarrow
(a) SBMNet \dagger	21.954	0.735	0.268
(b) w/o ISDM	21.401 $\downarrow_{0.553}$	0.726 $\downarrow_{0.009}$	0.285 $\uparrow_{0.017}$
(c) ISDM - SMU	21.635 $\downarrow_{0.319}$	0.728 $\downarrow_{0.007}$	0.279 $\uparrow_{0.011}$
(d) ISDM - IMU	21.732 $\downarrow_{0.222}$	0.730 $\downarrow_{0.005}$	0.281 $\uparrow_{0.013}$
(e) Bilinear	21.550 $\downarrow_{0.404}$	0.725 $\downarrow_{0.010}$	0.277 $\uparrow_{0.009}$
(f) RSMU - FSI	21.653 $\downarrow_{0.301}$	0.731 $\downarrow_{0.004}$	0.275 $\uparrow_{0.007}$

Table 5: Ablation of the ISDM and RSMU. The subscript for models (b-f) indicates the performance gap compared to the model (a). SBMNet \dagger denotes training w/o the loss term \mathcal{L}_{SL} .

Generalization Across Diverse Darkness Levels. *Figure 9* demonstrates the highly-robust generalization ability of our model across different levels of darkness. Its generalization is evident in maintaining excellent adaptability even under extremely short exposure conditions. In *Tables 1* and *2*, the 19-fold higher RMSE score compared to other methods also underscores the remarkable generalization of our approach across various darkness levels in images.

\mathcal{L}_{SL}	\mathcal{L}_{IS}	\mathcal{L}_R	\mathcal{L}_P	PSNR \uparrow	SSIM \uparrow	LPIPS \downarrow
	✓	✓	✓	21.954 $\downarrow_{0.310}$	0.735 $\downarrow_{0.008}$	0.268 $\uparrow_{0.014}$
✓	✓	✓		22.149 $\downarrow_{0.115}$	0.734 $\downarrow_{0.009}$	0.417 $\uparrow_{0.163}$
✓	✓	✓	✓	22.264	0.743	0.254

Table 6: Ablation of the different losses (\mathcal{L}_{SL} , \mathcal{L}_{IS} , and \mathcal{L}_P).

Computational Efficiency. To examine model efficiency, we reported the *Parameters(MB)* \downarrow , *FLOPs(G)* \downarrow and *Inference(S)* \downarrow of compared methods in *Table 3*. The measurements are conducted on a single 2080Titan GPU using images of size 128×128 . Our method achieves a good balance between performance and computational efficiency.

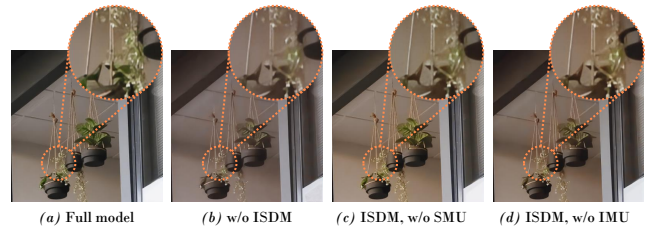


Figure 10: Ablation analysis with (w/) and without (w/o) the ISDM (also including the SMU, IMU components).

Ablation Study

Why Design the Dual-stream Learning Framework? As depicted in *Table 4*, removing the dual-stream branch and retaining only a single second-stage learning process results in a substantial 9% reduction in the most severe PSNR score degradation. Additionally, substituting the input of the second stage with x^{LL} leads to a decrease of 0.443 dB in PSNR. These observations collectively underscore the significance of applying prior constraints to low-light scenes.

Impact of ISDM. *Table 5* in [*Config. (b)-Config. (d)*] and *Figure 10* demonstrate the effectiveness of the ISDM module, including the efficacy of its intermediate components IMU and SMU. Compared to the baseline model [*Config. (a)*], removing the ISDM structure results in a significant performance drop (e.g., 0.553dB decrease in terms of PSNR). Similarly, removing its components (i.e., w/o SMU [*Config. (c)*] or [*Config. (d)*]) also leads to a decrease in performance. **Effects of RSMU.** *Table 5* in [*Config. (e)-Config. (f)*] presents the effectiveness of RSMU. In comparison to a simple up-sampling layer (e.g., Bilinear), RSMU facilitates a 0.404dB PSNR increase [*Config. (e)*]. The FSI module [*Config. (f)*] also contribute to the improvement in the final results.

Analysis of Different Losses. *Table 6* illustrates the ablation results for various loss components. We observe that the illuminance constraint (i.e., \mathcal{L}_{SL}) leads to an increase of 0.31 dB and 0.014 in PSNR and LPIPS scores, respectively. Additionally, the perceptual loss \mathcal{L}_P has the most significant impact on the perceptual LPIPS scores.

Conclusion and Remark

This study addresses the relatively unexplored challenge of super-resolution in ultra-dark environments. Leveraging a novel dual-modulated learning framework, we introduced specialized components to enhance feature-level preservation of illumination and color details, while mitigating artifacts through a resolution-sensitive merging up-sampler. Our approach’s remarkable applicability and generalizability across diverse ultra-low-light conditions were validated through comprehensive experiments. This work represents a significant advancement in addressing the complexities of super-resolution tasks under challenging low-light conditions.

Broader Impacts. Our work holds significance beyond the specific problem of ultra-dark super-resolution. This broader perspective reinvigorates the research landscape, encouraging exploration of joint multiple image processing tasks (i.e., low-light derain, low-light defog) in diverse adverse conditions.

References

- Aakerberg, A.; Nasrollahi, K.; and Moeslund, T. 2021. REL-LISUR: A Real Low-Light Image Super-Resolution Dataset. In Vanschoren, J.; and Yeung, S., eds., *Neural Information Processing Systems Track on Datasets and Benchmarks*, volume 1.
- Agaian, S. S.; Silver, B.; and Panetta, K. A. 2007. Transform coefficient histogram-based image enhancement algorithms using contrast entropy. *IEEE transactions on image processing*, 16(3): 741–758.
- Chen, X.; Wang, X.; Zhou, J.; Qiao, Y.; and Dong, C. 2023. Activating More Pixels in Image Super-Resolution Transformer. In *Computer Vision and Pattern Recognition*, 22367–22377.
- Deng, J.; Dong, W.; Socher, R.; Li, L.-J.; Li, K.; and Fei-Fei, L. 2009. Imagenet: A large-scale hierarchical image database. In *Computer Vision and Pattern Recognition*, 248–255. Ieee.
- Gao, J.; Liu, X.; Liu, R.; and Fan, X. 2023. Learning adaptive hyper-guidance via proxy-based bilevel optimization for image enhancement. *The Visual Computer*, 39(4): 1471–1484.
- Haris, M.; Shakhnarovich, G.; and Ukita, N. 2018. Deep back-projection networks for super-resolution. In *Computer Vision and Pattern Recognition*, 1664–1673.
- Hira, S.; Das, R.; Modi, A.; and Pakhomov, D. 2021. Delta Sampling R-BERT for limited data and low-light action recognition. In *Computer Vision and Pattern Recognition*, 853–862.
- Jiang, Y.; Gong, X.; Liu, D.; Cheng, Y.; Fang, C.; Shen, X.; Yang, J.; Zhou, P.; and Wang, Z. 2021. Enlightengan: Deep light enhancement without paired supervision. *IEEE transactions on image processing*, 30: 2340–2349.
- Johnson, J.; Alahi, A.; and Fei-Fei, L. 2016. Perceptual losses for real-time style transfer and super-resolution. In *Computer Vision–ECCV 2016: 14th European Conference, Amsterdam, The Netherlands, October 11–14, 2016, Proceedings, Part II 14*, 694–711. Springer.
- Li, C.; Guo, C.; and Loy, C. C. 2021. Learning to enhance low-light image via zero-reference deep curve estimation. *IEEE Transactions on Pattern Analysis and Machine Intelligence*, 44(8): 4225–4238.
- Li, M.; Liu, J.; Yang, W.; and Guo, Z. 2017. Joint denoising and enhancement for low-light images via retinex model. In *International Forum on Digital TV and Wireless Multimedia Communications*, 91–99. Springer.
- Li, Z.; Yang, J.; Liu, Z.; Yang, X.; Jeon, G.; and Wu, W. 2019. Feedback network for image super-resolution. In *Computer Vision and Pattern Recognition*, 3867–3876.
- Liang, J.; Cao, J.; Sun, G.; Zhang, K.; Van Gool, L.; and Timofte, R. 2021. Swinir: Image restoration using swin transformer. In *International Conference on Computer Vision*, 1833–1844.
- Liu, R.; Gao, J.; Zhang, J.; Meng, D.; and Lin, Z. 2021. Investigating bi-level optimization for learning and vision from a unified perspective: A survey and beyond. *IEEE Transactions on Pattern Analysis and Machine Intelligence*, 44(12): 10045–10067.
- Ma, L.; Liu, R.; Zhang, J.; Fan, X.; and Luo, Z. 2021. Learning deep context-sensitive decomposition for low-light image enhancement. *IEEE Transactions on Neural Networks and Learning Systems*, 33(10): 5666–5680.
- Ma, L.; Ma, T.; Liu, R.; Fan, X.; and Luo, Z. 2022. Toward fast, flexible, and robust low-light image enhancement. In *Computer Vision and Pattern Recognition*, 5637–5646.
- Mittal, A.; Soundararajan, R.; and Bovik, A. C. 2012. Making a “completely blind” image quality analyzer. *IEEE Signal processing letters*, 20(3): 209–212.
- Ren, X.; Yang, W.; Cheng, W.-H.; and Liu, J. 2020. LR3M: Robust low-light enhancement via low-rank regularized retinex model. *IEEE Transactions on Image Processing*, 29: 5862–5876.
- Wang, J.; Sun, K.; Cheng, T.; Jiang, B.; Deng, C.; Zhao, Y.; Liu, D.; Mu, Y.; Tan, M.; Wang, X.; et al. 2020. Deep high-resolution representation learning for visual recognition. *IEEE transactions on pattern analysis and machine intelligence*, 43(10): 3349–3364.
- Wang, R.; Zhang, Q.; Fu, C.-W.; Shen, X.; Zheng, W.-S.; and Jia, J. 2019. Underexposed photo enhancement using deep illumination estimation. In *Computer Vision and Pattern Recognition*, 6849–6857.
- Wang, S.; Zheng, J.; Hu, H.-M.; and Li, B. 2013. Naturalness preserved enhancement algorithm for non-uniform illumination images. *IEEE transactions on image processing*, 22(9): 3538–3548.
- Wang, T.; Zhang, K.; Shen, T.; Luo, W.; Stenger, B.; and Lu, T. 2023. Ultra-high-definition low-light image enhancement: A benchmark and transformer-based method. In *AAAI Conference on Artificial Intelligence*, volume 37, 2654–2662.
- Wang, W.; Wei, C.; Yang, W.; and Liu, J. 2018a. Gladnet: Low-light enhancement network with global awareness. In *International conference on automatic face & gesture recognition*, 751–755. IEEE.
- Wang, X.; Yu, K.; Wu, S.; Gu, J.; Liu, Y.; Dong, C.; Qiao, Y.; and Change Loy, C. 2018b. Esrgan: Enhanced super-resolution generative adversarial networks. In *Proceedings of the European conference on computer vision (ECCV) workshops*, 0–0.
- Wei, C.; Wang, W.; Yang, W.; and Liu, J. 2018. Deep retinex decomposition for low-light enhancement. *arXiv preprint arXiv:1808.04560*.
- Yang, W.; Wang, S.; Fang, Y.; Wang, Y.; and Liu, J. 2020a. From fidelity to perceptual quality: A semi-supervised approach for low-light image enhancement. In *Computer Vision and Pattern Recognition*, 3063–3072.
- Yang, W.; Yuan, Y.; Ren, W.; Liu, J.; Scheirer, W. J.; Wang, Z.; Zhang; and et al. 2020b. Advancing Image Understanding in Poor Visibility Environments: A Collective Benchmark Study. *IEEE Transactions on Image Processing*, 29: 5737–5752.
- Zamir, S. W.; Arora, A.; Khan, S.; Hayat, M.; Khan, F. S.; and Yang, M.-H. 2022a. Restormer: Efficient transformer for high-resolution image restoration. In *Computer Vision and Pattern Recognition*, 5728–5739.

Zamir, S. W.; Arora, A.; Khan, S.; Hayat, M.; Khan, F. S.; Yang, M.-H.; and Shao, L. 2020. Learning enriched features for real image restoration and enhancement. In *European Conference on Computer Vision*, 492–511.

Zamir, S. W.; Arora, A.; Khan, S. H.; Munawar, H.; Khan, F. S.; Yang, M.-H.; and Shao, L. 2022b. Learning Enriched Features for Fast Image Restoration and Enhancement. *IEEE Transactions on Pattern Analysis and Machine Intelligence*.

Zhang, Y.; Li, K.; Li, K.; Wang, L.; Zhong, B.; and Fu, Y. 2018a. Image super-resolution using very deep residual channel attention networks. In *European conference on computer vision*, 286–301.

Zhang, Y.; Tian, Y.; Kong, Y.; Zhong, B.; and Fu, Y. 2018b. Residual dense network for image super-resolution. In *Computer Vision and Pattern Recognition*, 2472–2481.

Zhang, Y.; Zhang, J.; and Guo, X. 2019. Kindling the darkness: A practical low-light image enhancer. In *ACM international conference on multimedia*, 1632–1640.

Zhao, H.; Kong, X.; He, J.; Qiao, Y.; and Dong, C. 2020. Efficient image super-resolution using pixel attention. In *European Conference on Computer Vision*, 56–72.

Zhou, Y.; Li, Z.; Guo, C.-L.; Bai, S.; Cheng, M.-M.; and Hou, Q. 2023. SRFormer: Permuted Self-Attention for Single Image Super-Resolution. *arXiv preprint arXiv:2303.09735*.